Tuning the robust magnetic properties in MPS_3 (M = Mn, Fe, and Ni) by proximity-induced Dzyaloshinskii-Moriya interactions

Suvodeep Paul,[1,*] Devesh Negi,[1] Saswata Talukdar,[1] Saheb Karak,[1] Shalini Badola,[1] Bommareddy Poojitha,[1] Manasi Mandal,[1] Sourav Marik,[1] R. P. Singh,[1] Nashra Pistawala,[2] Luminita Harnagea,[3] Aksa Thomas,[4] Ajay Soni,[4] Subhro Bhattacharjee,[5] and Surajit Saha[1,†]

[1]*Department of Physics, Indian Institute of Science Education and Research Bhopal, Bhopal 462066, Madhya Pradesh, India*
[2]*Department of Physics, Indian Institute of Science Education and Research Pune, Pune 411008, Maharashtra, India*
[3]*I-HUB Quantum Technology Foundation, Indian Institute of Science Education and Research Pune, Pune 411008, Maharashtra, India*
[4]*School of Physical Sciences, Indian Institute of Technology, Mandi 175005, Himachal Pradesh, India*
[5]*International Centre for Theoretical Sciences, Tata Institute of Fundamental Research, Bangalore 560089, India*

(Received 5 September 2023; revised 11 November 2023; accepted 22 January 2024; published 23 February 2024)

We have demonstrated the possibility to control the otherwise robust magnetic properties of transition-metal phosphorus trisulfides (Mn/Fe/$NiPS_3$) in their heterostructures with Weyl semimetallic $MoTe_2$ which can be attributed to the Dzyaloshinskii-Moriya (DM) interactions at the interface of the two materials. While the DM interaction is known to scale with the strength of the spin-orbit coupling (SOC), we demonstrate using experiments on heterostructures with a variety of substrates (underlayers) hosting variable SOC and electronic density of states (DOS) that the effect of DM interaction strongly varies with the electronic DOS of the SOC-hosting layer as well as the spin orientation and degree of anisotropy associated with the magnetic layer.

DOI: 10.1103/PhysRevB.109.085136

I. INTRODUCTION

Controlling the quantum many-body interactions is the key to discovering emergent phenomena and exploring potential technological applications. This may be achieved by the influence of various stimuli like the effect of reduced dimensionality [1], the application of an electric or a magnetic field [2], ultrafast laser pulses [3], proximity to suitable substrates, etc. [4,5]. The proximity effect, in two-dimensional (2D) layered materials, may be induced by creating appropriate heterostructures. Engineered heterostructures of 2D materials is one of the ways to effectively control the quantum many-body interactions. The 2D layered magnets exhibit novel magnetic properties wherein heterostructure engineering could introduce effects of broken-inversion symmetry as well as spin-orbit and Dzyaloshinskii-Moriya (DM) interactions, thus resulting in new exotic ground states. Examples of such ground states are topologically protected spin textures like skyrmions and chiral domain walls [6–10], which can have novel spin-orbitronic and storage applications [11,12].

Transition-metal phosphorus trisulfides (MPS_3, M = Mn, Fe, and Ni) are a class of such van der Waals materials that host antiferromagnetic (AFM) ground states at low temperatures [13,14]. The AFM ground state exhibits different spin dimensionalities (viz., $n = 1$, 2, and 3) due to the presence of an axial or planar anisotropy or in the absence of any anisotropic element [15] which may be described by the Ising (e.g., $FePS_3$), XY (e.g., $NiPS_3$), and Heisenberg (e.g., $MnPS_3$) Hamiltonians, respectively [13]. Engineered heterostructures of magnetic layered materials with high spin-orbit coupled systems like topological materials have the potential to control the quantum interactions, unraveling a variety of exotic phenomena at their interfaces [4,16,17]. We have performed a comprehensive study on the heterostructures of various MPS_3 compounds (M = Mn, Fe, and Ni) with the topological Weyl semimetal T_d-$MoTe_2$ that serves as an excellent platform for exploring the rich interfacial phenomena like the Rashba effect, DM interactions, and the effect of spin orientations and dimensionalities on their properties.

Raman spectroscopy is a nondestructive characterizing tool for low-dimensional crystals that can provide information about the sample's structure, phonon properties, couplings between the various degrees of freedom, and many-body interactions involving low-energy excitations [18–20]. The magnetic ordering in a material affects the phonon properties due to spin-phonon interactions [3,21] or magnetoelastic couplings, and these signatures can be observed through Raman scattering. Therefore, Raman measurements are very well suited for the detection of spin ordering in low-dimensional magnets [22–24], especially, for micrometer-sized flakes and heterostructures where standard bulk measurement techniques like superconducting quantum interference device–vibrating-sample magnetometer are not very suitable.

Here, we bring out the robustness [22–24] of the magnetic ordering in MPS_3 compounds (M = Mn, Fe, and Ni) to flake thickness. Our measurements on $MPS_3/MoTe_2$ heterostructures demonstrate a strong suppression of the magnetic ordering for $MnPS_3$ and $FePS_3$, whereas no observable effects on $NiPS_3$, which could have its origin in the spin, orbit, and charge couplings at the interface mediated by DM

*Corresponding author: suvodeeppaul100@gmail.com
†Corresponding author: surajit@iiserb.ac.in

interactions. More importantly, the interfacial interactions reveal strong sensitivity to the low-energy electronic density of states of the nonmagnetic layer (substrate or underlayer) as well as the orientation of the spins and the degree of magnetic anisotropy in the magnetic layer. Our observations are supported by extensive experiments on heterostructures of MPS$_3$ with Sb_2Te_3, Au, and Cu with varying spin-orbit coupling (SOC) and electronic density of states.

II. EXPERIMENTAL DETAILS

Single crystals of $MnPS_3$, $FePS_3$, and $NiPS_3$ were micromechanically exfoliated using the standard Scotch tape technique to obtain thin nanoflakes of the materials on SiO_2/Si substrates. Additionally, heterostructures with $MoTe_2$ and Sb_2Te_3 (on SiO_2/Si substrate) were prepared by a dry transfer technique under a microscope using a custom-built 2D transfer system. Further, gold- and copper-supported samples were also prepared by the similar standard micromechanical exfoliation technique on the substrates of SiO_2/Si predeposited with Au and Cu, respectively. A detailed description of the various samples and their preparation is added in the Supplemental Material [25] (see Note 1 and Fig. S1). The corresponding thicknesses of the samples have been determined through atomic force microscopy measurements shown in Supplemental Material [25] (Note 1, Figs. S2–S8). Raman measurements were performed using a HORIBA HR Evolution spectrometer with a 532-nm excitation laser. Low-temperature measurements were performed in a LINKAM heating stage for the $NiPS_3$ samples, and in a closed-cycle He cryostat (AttoDRY 1000) for the $MnPS_3$ and $FePS_3$ samples.

III. RESULTS

The MPS$_3$ compounds possess a monoclinic crystal structure, as shown in Fig. 1(a), with a space group of $C2/m$ [26,27]. The transition-metal M atoms form a honeycomb structure where each M atom is coordinated to 6 S atoms in a trigonal symmetry, thereby forming an MS$_6$ octahedron with its trigonal axis perpendicular to the basal plane of the crystal. The S atoms are further bonded to 2 P atoms above and below the M plane arranged in the shape of a dumbbell.

The MPS$_3$ compounds undergo a transition from the paramagnetic (PM) to the AFM phase, as reported earlier [13], at the corresponding Néel temperatures (T_N's) of 80, 115, and 150 K for $MnPS_3$, $FePS_3$, and $NiPS_3$, respectively, as can be seen from their magnetization data shown in Fig. 1(b) (see Note 2 of Supplemental Material [25] for more details). Though the MPS$_3$ compounds are isostructural, they exhibit contrasting spin structures in their respective AFM phases, as shown in Figs. 1(c)–1(e), middle panels, based on the choice of transition-metal atom (Mn, Fe, or Ni). Both $MnPS_3$ and $FePS_3$ have their magnetic moments oriented out of plane (parallel to the trigonal axis of the MS$_6$ octahedra) [28–30]. $NiPS_3$, on the other hand, has all the magnetic moments oriented in plane (perpendicular to the trigonal axis of the MS$_6$ octahedra) along the a axis in its AFM phase [31]. Furthermore, while $MnPS_3$ shows antiferromagnetic ordering with respect to the nearest neighbors in the honeycomb lattice formed by the Mn^{2+} ions, $FePS_3$ and $NiPS_3$ give the appearance of two antiferromagnetically ordered chains of ferromagnetically ordered Fe^{2+}/Ni^{2+} ions [26,28,31,32]. However, unlike $NiPS_3$ (and $MnPS_3$), $FePS_3$ exhibits unidentical magnetic and crystallographic unit cells [28].

The AFM transition in the MPS$_3$ compounds has been reported to result in spin-lattice coupling of selected phonons across the T_N [14,22–24]. The Raman spectra of all three compounds are nearly identical in their paramagnetic phase, recorded at 300 K [refer to Figs. 1(c)–1(e), top panels)]. The modes are labeled as M_1–M_8 (for $MnPS_3$), F_1–F_6 (for $FePS_3$), and N_1–N_{10} (for $NiPS_3$), respectively. Some of these modes respond to the antiferromagnetic transitions of MPS$_3$ (M = Mn, Fe, and Ni) at low temperatures. The most prominent Raman signatures of these AFM transitions are depicted in the bottom panels of Figs. 1(c)–1(e). The M_2 phonon [Fig. 1(c), bottom panel] of $MnPS_3$ shifts from $\sim$156 cm^{-1} in the PM phase (represented by white vertical dashed line) to $\sim$151 cm^{-1} in the AFM phase (represented by blue vertical dashed line). While for $FePS_3$, the F_1 mode [Fig. 1(d), bottom panel] splits into sharp peaks (F_{1a} and F_{1b}) below the T_N [22], in $NiPS_3$, the N_2 mode [Fig. 1(e), bottom panel] shows a clear departure from the anharmonic behavior below T_N due to spin-phonon coupling. The onset of the spin-phonon coupling is identified as the AFM spin-ordering temperature [33]. For a detailed description of these features and additional evidence of the AFM transition using Raman measurements, refer to Note 2 of the Supplemental Material [25].

Figure 2 shows the AFM ordering temperature for various flakes and heterostructures of $MnPS_3$, an isotropic Heisenberg magnet. From the contour maps in Fig. 2(a), it can be clearly observed that the AFM ordering takes place at $\sim$80 K for all four flakes of $MnPS_3$ of different thicknesses (250, 118, 14, and 5 nm, respectively) supported on SiO_2/Si substrate (Note 2 in Supplemental Material [25]). This is consistent with various recent experimental and theoretical reports [24,34]. The weak dependence of the T_N on the flake thickness may be attributed to the weak interlayer coupling in $MnPS_3$ [32]. We have investigated the heterostructures of $MnPS_3$ with $MoTe_2$, which transforms to the T_d phase, a Weyl semimetallic phase, at low temperatures below $\sim$250 K [35–37] (Note 3 in the Supplemental Material [25]). It is interesting to see that the proximity to the Weyl semimetallic T_d-$MoTe_2$ suppresses the T_N of the $MnPS_3$ flakes considerably. Further, it is also observed that the suppression is different for different thicknesses of $MnPS_3$. The bulk exfoliated flake of $MnPS_3$ of thicknesses $\sim$300 nm shows a suppression of the T_N from $\sim$80 to $\sim$35 K, while for the 144-nm-thick flake, the T_N shifts down to below 5 K, in the corresponding heterostructures with T_d-$MoTe_2$. For the $MnPS_3$ flake of thickness $\sim$14 nm on T_d-$MoTe_2$, the Raman signatures are too weak to resolve due to its lower cross section (as shown in Fig. S16 of Supplemental Material [25]). Nonetheless, the data on the $\sim$14-nm-thick flake suggest a complete suppression of the AFM phase. (See Note 4 in the Supplemental Material [25].) In order to understand the origin of the suppression, we have further performed experiments on $MnPS_3$ heterostructures with a range of different underlayers of topological and nontopological materials with a wide variety of SOC strengths and electronic density of states. The results obtained are summarized in Fig. 2(b). While experi-

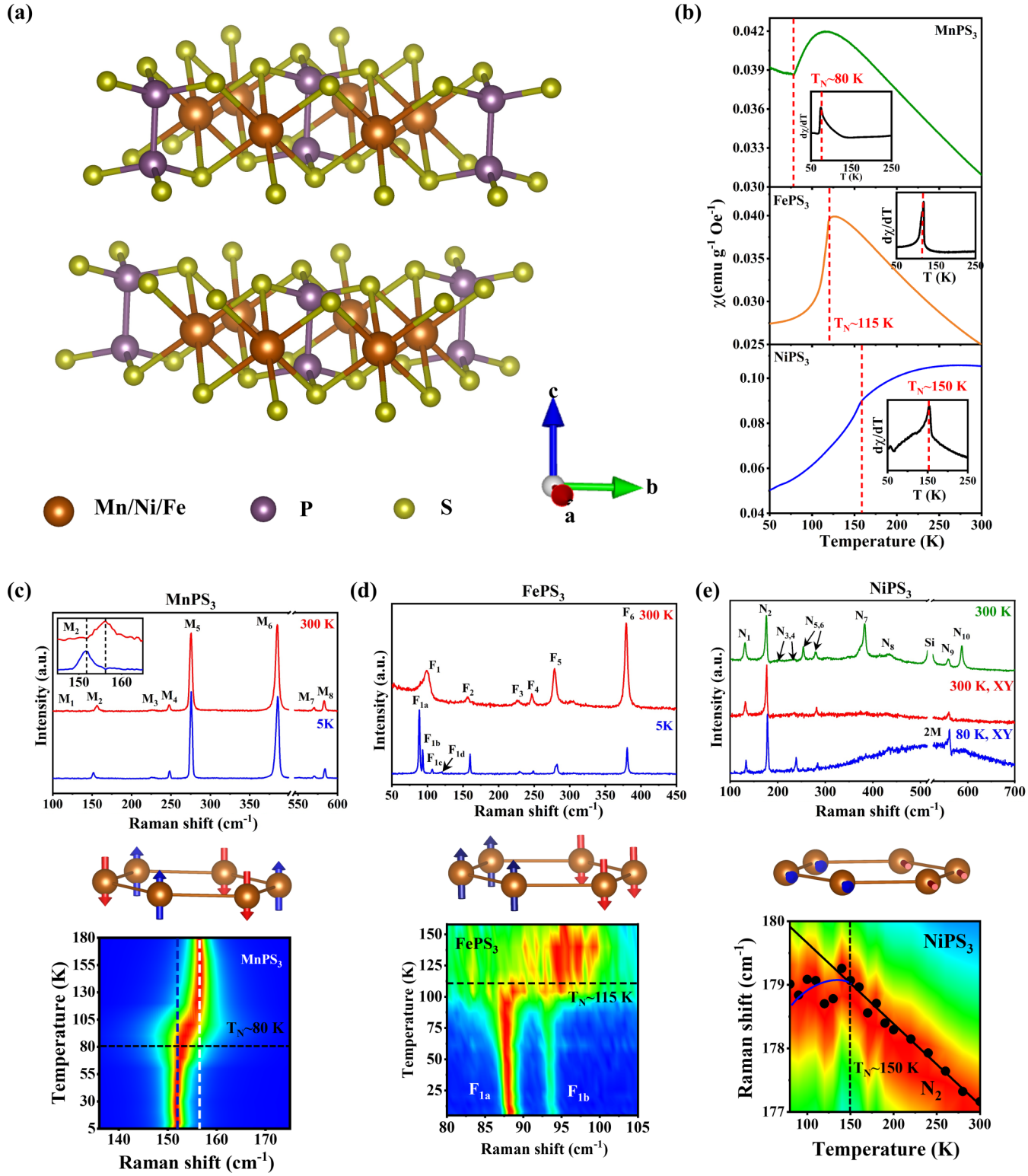

FIG. 1. (a) The crystal structure of MPS_3 (M = Mn, Fe, and Ni). (b) The temperature variation of magnetic susceptibilities (χ) and the respective temperature derivatives ($d\chi/dT$) (shown in insets; unit: emu g^{-1} Oe^{-1} K^{-1}) for $MnPS_3$, $FePS_3$, and $NiPS_3$ bulk single crystals. (c)–(e) The Raman spectra obtained in the paramagnetic and antiferromagnetic phases of MPS_3 (M = Mn, Fe, and Ni). The spin structures in the AFM phase and the most prominent Raman signatures are shown below the corresponding Raman spectra.

ments performed on flakes of varying thickness directly on SiO_2/Si substrate showed no change from the reported bulk T_N value ~80 K, strong suppression was observed for all the flakes supported on T_d-$MoTe_2$ (type-II Weyl semimetal with strong SOC), Sb_2Te_3 (topological insulator with strong SOC), gold (metallic with strong atomic SOC), and copper (metallic with poor atomic SOC). Furthermore, the suppression was observed to be stronger for thinner flakes of $MnPS_3$.

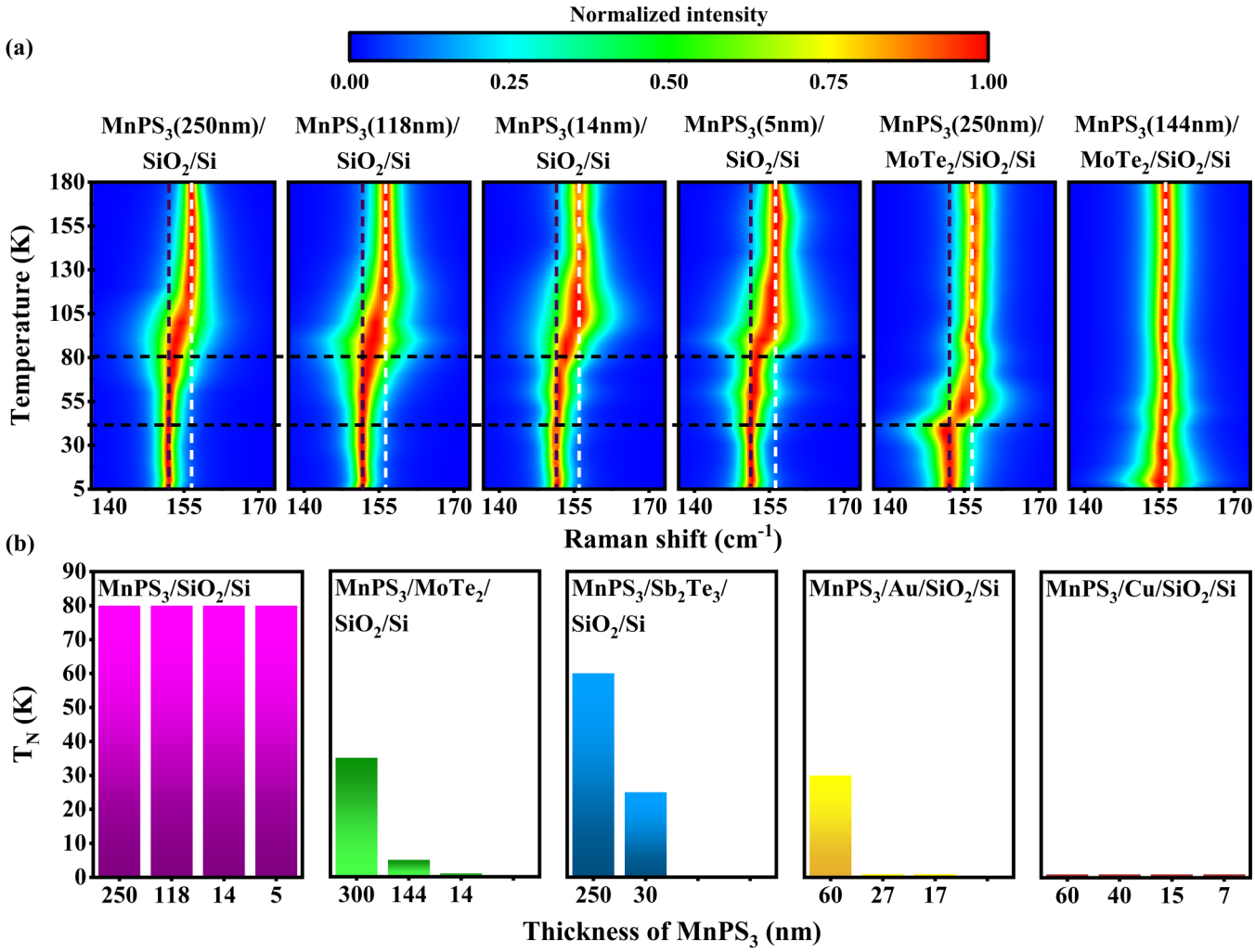

FIG. 2. (a) The color maps show the intensity profile of the M_2 phonon across the magnetic phase transition for $MnPS_3$ flakes of various thickness on SiO_2/Si substrate and in heterostructures with T_d-$MoTe_2$. The dashed horizontal lines mark the corresponding Néel temperatures. (b) The obtained Néel temperatures of $MnPS_3$ in heterostructures of various thicknesses of $MnPS_3$ with varying underlayers (substrates) (SiO_2/Si, $MoTe_2$, Sb_2Te_3, Au, and Cu).

Figure 3(a) shows the contour maps corresponding to two different thicknesses of $FePS_3$ (Ising-type AFM) on SiO_2/Si substrate and two heterostructures with T_d-$MoTe_2$ as underlayer. It can be clearly observed that the T_N (temperature where the F_{1a} and F_{1b} features disappear and the asymmetric F_1 mode appears instead) for $FePS_3$ flakes of thickness ∼50 and ∼10 nm on SiO_2/Si substrate are measured to be ∼110 K, again pointing out its insensitivity to the flake thickness. The heterostructures of $FePS_3$ and T_d-$MoTe_2$ with two different thicknesses (∼50 and ∼23 nm) of the $FePS_3$ layers exhibited a suppression of the T_N to ∼80 K for the 50-nm-thick flake of $FePS_3$ and to ∼75 K for the 23-nm flake on T_d-$MoTe_2$. This is consistent with the observation of suppression of T_N in $MnPS_3$.

Figure 3(b) shows the temperature dependence of the N_2 mode of $NiPS_3$ (an *XY*-type AFM), for various flakes and corresponding heterostructures with T_d-$MoTe_2$. The flakes of thicknesses 44, 33, and 12 nm supported on SiO_2/Si substrate exhibit T_N of ∼150 K, implying its invariance with the thickness. It is interesting to observe that unlike $MnPS_3$ and $FePS_3$, the introduction of T_d-$MoTe_2$ underlayers shows no considerable changes in the magnetic ordering temperature (T_N) with respect to the flakes directly on the SiO_2/Si substrate. The observations on $NiPS_3$ are in sharp contrast to those in the case of $MnPS_3/FePS_3$ discussed above.

IV. DISCUSSION

Our primary observations are (i) the strong suppression of the AFM phase of $MnPS_3$ and $FePS_3$ in their heterostructures with T_d-$MoTe_2$ which are otherwise robust to their flake thickness, while (ii) the AFM phase in $NiPS_3$ remains robust even in its heterostructures with T_d-$MoTe_2$. We will now discuss these findings and their possible origin.

As predicted by Mermin-Wagner-Hohenberg theorem [38,39], magnetic ordering is prohibited in 2D isotropic Heisenberg magnets. However, the presence of magnetocrystalline anisotropy in the 2D MPS_3 systems brings magnetic ordering into existence, as discussed in Note 5 of the Supplemental Material [25,40]. It may be noted that Neal *et al.* [41,42] have recently demonstrated an intriguing symmetry crossover from $C2/m$ to $P\bar{3}1m$ in Mn/$FePS_3$, but absent in

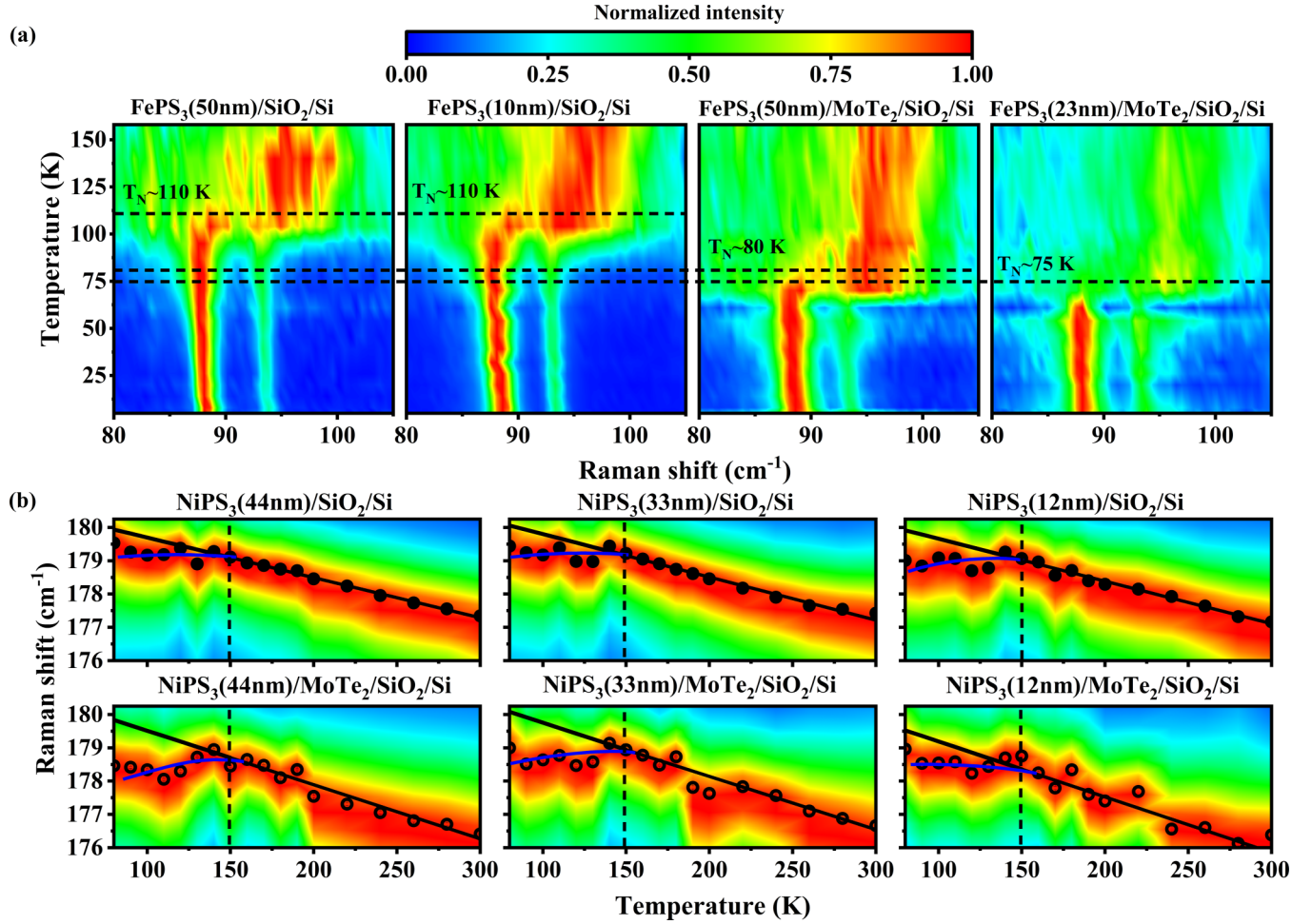

FIG. 3. (a) The color maps show the intensity profile of the F_1 phonon across the magnetic phase transition for $FePS_3$ flakes of various thickness on SiO_2/Si substrate and in heterostructures with T_d-$MoTe_2$. The dashed horizontal lines mark the corresponding Néel temperatures. (b) The color maps show the intensity profile of the N_2 phonon across the magnetic phase transition for $NiPS_3$ flakes of various thickness on SiO_2/Si substrate and in heterostructures with T_d-$MoTe_2$. The N_2 phonon clearly shows deviations (represented by solid blue line) from anharmonic trend (represented by solid black lines). The onsets of the deviations are measured as the Néel temperatures for the corresponding flakes of $NiPS_3$ and are marked by the dashed vertical lines.

$NiPS_3$, as the crystals are thinned down from bulk to thin layers. However, such a symmetry crossover was observed to have no relation to the magnetic ordering phenomena as is evident from the thickness insensitivity of the Néel temperatures for all three compounds [22–24]. Chittari *et al.* [43] using *ab initio* calculations have predicted a transition from the semiconducting AFM to a metallic FM phase in MPS_3 compounds by means of charge doping and application of strain. While the coupling between the magnetic layer and the $MoTe_2$ underlayer in the reported heterostructures is strong (refer to Supplemental Material [25], Note 7 and Ref. [44]), the required charge doping for a transition from the semiconducting AFM to a metallic FM phase is of the order of $\sim 10^{14}\,\mathrm{cm}^{-2}$ [43], which is unlikely to be achieved by mere diffusion across the interfaces with the underlayers (substrates) in the absence of a strong bias voltage (as is the case in our experiments). On the other hand, the application of strain is typically expected to result in frequency shifts of phonons with respect to the unstrained phonons. Notably, our experiments show no appreciable shift in the phonon frequencies or any dependence on the $MnPS_3$ flake thickness (Fig. S17 in Supplemental Material [25]). Therefore, possibilities like reduced dimensionality, symmetry crossover, charge doping, and strain may be ruled out in our experiments, as discussed further in Supplemental Material [25] (Notes 5 and 6 and Figs. S17 and S18). Instead, we argue that the DM interaction arising from the SOC of the underlying substrate is the principal driving mechanism.

The magnetic interactions between neighboring spins of the MPS_3 compounds may be described by the following Hamiltonian [13]:

$$H = -2\sum\left\{J_{\perp}(S_{ix}S_{jx} + S_{iy}S_{jy}) + J_{\parallel}(S_{ix}S_{jx} + S_{iy}S_{jy}) + AS_{iz}^2\right\} + H_{\mathrm{DM}}, \quad (1)$$

$$H_{\mathrm{DM}} = \boldsymbol{D_{ij}}.(\boldsymbol{S_i} \times \boldsymbol{S_j}). \quad (2)$$

Here, $J_{\perp}$ and $J_{||}$ represent the perpendicular and parallel exchange interactions between the spins $\boldsymbol{S_i}$ and $\boldsymbol{S_j}$, while A represents the single-ion anisotropy induced by the axial distortion. The last term in Eq. (1) captures the

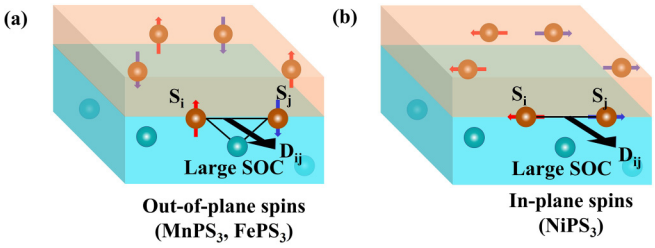

FIG. 4. Schematic representation of the Dzyaloshinskii-Moriya interactions in (a) magnetic thin films with spins oriented out of plane (e.g., $MnPS_3$ and $FePS_3$) and (b) magnetic thin films with spins oriented in plane (e.g., $NiPS_3$).

Dzyaloshinskii-Moriya (DM) interaction and is expanded in Eq. (2). While the first two terms support a collinear arrangement of neighboring spins, the H_{DM} prefers a perpendicular arrangement [11,45,46]. However, a nonzero DM interaction requires SOC as well as the absence of inversion symmetry.

The bulk $M\mathrm{PS}_3$ (M = Mn, Fe, and Ni) crystals, on account of their monoclinic structures, preserve the inversion symmetry and, therefore, DM interactions are absent. However, the exfoliated thin flakes of $M\mathrm{PS}_3$ break the inversion symmetry at their interfaces and are ideal platforms to introduce DM interactions [11]. In particular, the breaking of inversion symmetry at the interface of a heterojunction can give rise to momentum-dependent spin split dispersions as a consequence of Dresselhaus- or Rashba-type SOC [11,47], which in turn lead to significant DM interactions at the interfaces of magnetic heterojunctions [48,49], particularly in the presence of low-energy charge carriers, i.e., in metallic and semimetallic substrate. Recent angle-resolved photoemission spectroscopy measurements revealed that Au and Cu possess Rashba SOC [50,51]. Furthermore, the topological substrates (underlayers) T_d-MoTe_2 and $\mathrm{Sb}_2\mathrm{Te}_3$ inherently host strong SOC. Therefore, in all our measurements on the thin flakes of $M\mathrm{PS}_3$ (M = Mn, Fe, and Ni) supported on underlayers (substrates) of T_d-MoTe_2, $\mathrm{Sb}_2\mathrm{Te}_3$, Au, and Cu, due to the broken-inversion symmetry and the presence of SOC, the DM interaction must be introduced at their interfaces. This is very significant as the DM interaction is supposed to be dominant at the vicinity of the interface (where the inversion symmetry is broken), thereby introducing a plausible dependence of the magnetic interactions on the flake thickness. The competition between Heisenberg and DM interaction terms induces a canting of the perfectly antiparallel spins in an AFM [Fig. 4(a)], resulting in weakening of the AFM ordering, thereby explaining the suppression of the AFM phase in the investigated Mn/FePS_3 thin flakes. It is important to note that the DM interactions would be dominant for the spins in the vicinity of the interface with the nonmagnetic layer and not necessarily in the entire bulk of the flake. Notably, we can rule out the contribution of Ruderman-Kittel-Kasuya-Yosida (RKKY) effect, mediated through free carriers, on the DM interactions due to the wide-gap semiconducting nature of $M\mathrm{PS}_3$ [43]. Interestingly, few recent studies have reported the magnetic properties and ordering temperatures in AFMs to be strongly affected by modifications of the surface magnetism [52–54]. The DM interactions in our experiments similarly affect the magnetic ordering at the interfacial surface of the magnetic layer, which in turn is likely to affect the magnetic ground state of the entire bulk flake. An exact calculation of the surface magnetism effects on the magnetic properties is crucial to shed further light on the mechanism, which is beyond the scope of this work.

Our results also bring out certain traits of the interfacial DM interactions observed in the 2D magnetic $M\mathrm{PS}_3$ thin films, as explained next.

A. Effect of spin orientation associated with the magnetic layer

The DM interaction energy between two spins $\boldsymbol{S}_i$ and $\boldsymbol{S}_j$, as described by Eq. (2), clearly invokes a dependence on the spin orientations. For the heterostructures, the DM vector $\boldsymbol{D}_{ij}$ $(= -\boldsymbol{D}_{ji}) = \boldsymbol{n} \times \boldsymbol{r}_{ij}$ lies in the plane of the interface between the magnetic and the nonmagnetic layer, while $\boldsymbol{n}$ and $\boldsymbol{r}_{ij}$ are the normal to the interface and the distance between the spins, $\boldsymbol{S}_i$ and $\boldsymbol{S}_j$, respectively [11]. It is evident from the above expression that the DM interactions would be drastically different for the out-of-plane and the in-plane spins, as illustrated schematically in Fig. 4. While for the out-of-plane spins, the DM interactions result in the canting of the spins towards each other along a direction perpendicular to their separation ($\boldsymbol{r}_{ij}$) and the normal ($\boldsymbol{n}$) to the surface, the DM interactions would vanish for the in-plane spins (which are coplanar with the $\boldsymbol{D}_{ij}$ vector). This explains why the introduction of T_d-MoTe_2 suppresses the AFM ordering temperature for MnPS_3 and FePS_3 (spins oriented out of plane), while NiPS_3 (spins oriented in plane) remains unaffected. Interestingly, while we observe a complete suppression of AFM phase for flakes of appreciably thick (∼144 nm) MnPS_3 layers, the FePS_3 flakes of relatively thinner (∼23 nm) layers do not undergo a complete suppression of the AFM phase upon incorporation of the MoTe_2 underlayer. This may be attributed to the fact that MnPS_3 exhibits a nearly isotropic Heisenberg-type interaction ($J_{\parallel} = J_{\perp}$), while FePS_3 shows an anisotropic Ising-type behavior ($J_{\parallel} \neq J_{\perp}$) [13]. Therefore, randomization of the spins in MnPS_3 would cost less energy as compared to FePS_3, which has a stronger out-of-plane anisotropy. As opposed to the results obtained for MnPS_3 and FePS_3, we observed that NiPS_3 flakes (which have their spins oriented in plane) showed no appreciable changes in the T_{N} in the heterostructures with T_d-MoTe_2.

B. Effect of the density of electronic states in the nonmagnetic underlayer

We also observe that despite having similar thicknesses (∼60 nm), the MnPS_3 flake on Cu shows stronger suppression of AFM ordering compared to a similarly thick flake on Au [Fig. 2(b)]. This we attribute to the higher density of states associated with Cu as compared to Au [55]. Given the substantial suppression on Cu substrate (with negligible atomic SOC) as well as Au (with substantial atomic SOC), we think the electronic density of states plays the primary role in the suppression of the magnetic interactions as compared to the spin-orbit coupling.

V. CONCLUSION

In summary, we have prepared heterostructures of van der Waals antiferromagnet MPS_3 (M = Mn, Fe, and Ni) with T_d-$MoTe_2$, Sb_2Te_3, Au, and Cu. We have observed (i) a layer-dependent suppression of the otherwise robust magnetic ordering which has been attributed to the presence of strong DM interactions at the interface, (ii) the strength of DM interactions varies with (a) the low-energy electronic density of states of the SOC-hosting nonmagnetic underlayer, and (b) the spin orientation and the degree of anisotropy associated with the antiferromagnetic overlayer. We believe that our extensive study will be vital to create tailor-made magnetic states through interface engineering for potential spintronic and spin-orbitronic applications.

ACKNOWLEDGMENTS

S.S. acknowledges funding from the Science and Engineering Research Board (SERB), India (Grants No. ECR/2016/001376 and No. CRG/2019/002668) and Ministry of Education, India (Grant No. STARS/APR2019/PS/662/FS). D.N. received support from a CSIR fellowship (No. 09/1020/(0139)/2018-EMR-I). The authors acknowledge Physics PG laboratory and Central Instrumentation Facility (IISER Bhopal) for thermal evaporation and sputtering facilities. L.H. acknowledges financial support from DST-India [Grant No. DST/WOS-A/PM-83/2021 (G)] and National Mission on Interdisciplinary Cyber-Physical Systems (NM-ICPS) of the Department of Science and Technology, Government Of India through the I-HUB Quantum Technology Foundation, Pune, India. R.P.S. acknowledges fundings from DST/SERB (Grant No. YSS/2015/001799). A.S. acknowledges IIT Mandi for research facilities. S.B. received support from the adjunct fellow program at SNBNCBS, Kolkata, and funding from Max Planck partner group grant at ICTS, SERB-DST (India) for Swarna Jayanti Grant No. SB/SJF/2021-22/12-G and the Department of Atomic Energy, Government of India, under Project No. RTI4001.

S.P. and S.S. conceived the idea; N.P. and L.H. were involved in the synthesis of the $FePS_3$ single crystals, while M.M., S.M., and R.P.S. were involved in the synthesis of the $MoTe_2$ single crystals; the exfoliated thin films of various MPS_3 compounds and their heterostructures were prepared by S.P., D.N., and S.T.; Raman measurements were performed by S.P., D.N., S.T., S.K., and B.P; atomic force microscopy measurements were performed by A.T. and A.S., all data analysis and data interpretation were done by S.P.; magnetic measurements were performed by S.P., D.N., and S. Badola. The manuscript was written by S.P., S.S., and Subhro Bhattacharjee in consultation with all the authors.

The authors declare no competing financial interests.

[1] Y. Deng, Y. Yu, Y. Song, J. Zhang, N. Z. Wang, Z. Sun, Y. Yi, Y. Z. Wu, S. Wu, and J. Zhu, Gate-tunable room-temperature ferromagnetism in two-dimensional Fe_3GeTe_2, Nature (London) **563**, 94 (2018).

[2] D. Vaclavkova, M. Palit, J. Wyzula, S. Ghosh, A. Delhomme, S. Maity, P. Kapuscinski, A. Ghosh, M. Veis, and M. Grzeszczyk, Magnon polarons in the van der Waals antiferromagnet $FePS_3$, Phys. Rev. B **104**, 134437 (2021).

[3] F. Mertens, D. Mönkebüscher, U. Parlak, C. Boix-Constant, S. Mañas-Valero, M. Matzer, R. Adhikari, A. Bonanni, E. Coronado, and A. M. Kalashnikova, Ultrafast coherent THz lattice dynamics coupled to spins in the van der Waals antiferromagnet $FePS_3$, Adv. Mater. **35**, 2208355 (2023).

[4] H. Wang, Y. Liu, P. Wu, W. Hou, Y. Jiang, X. Li, C. Pandey, D. Chen, Q. Yang, and H. Wang, Above room-temperature ferromagnetism in wafer-scale two-dimensional van der Waals Fe_3GeTe_2 tailored by a topological insulator, ACS Nano **14**, 10045 (2020).

[5] S. Zhang, R. Xu, N. Luo, and X. Zou, Two-dimensional magnetic materials: Structures, properties and external controls, Nanoscale **13**, 1398 (2021).

[6] S. Mühlbauer, B. Binz, F. Jonietz, C. Pfleiderer, A. Rosch, A. Neubauer, R. Georgii, and P. Böni, Skyrmion lattice in a chiral magnet, Science **323**, 915 (2009).

[7] M. Heide, G. Bihlmayer, and S. Blügel, Dzyaloshinskii-Moriya Interaction Accounting for the Orientation of Magnetic Domains in Ultrathin Films: Fe/W (110), Phys. Rev. B **78**, 140403(R) (2008).

[8] S. Kim, K. Ueda, G. Go, P.-H. Jang, K.-J. Lee, A. Belabbes, A. Manchon, M. Suzuki, Y. Kotani, and T. Nakamura, Correlation of the Dzyaloshinskii–Moriya interaction with heisenberg exchange and orbital asphericity, Nat. Commun. **9**, 1648 (2018).

[9] M. R. K. Akanda, I. J. Park, and R. K. Lake, Interfacial dzyaloshinskii-moriya interaction of antiferromagnetic materials, Phys. Rev. B **102**, 224414 (2020).

[10] Y. Wu, S. Zhang, J. Zhang, W. Wang, Y. L. Zhu, J. Hu, G. Yin, K. Wong, C. Fang, and C. Wan, Néel-type Skyrmion in WTe_2/Fe_3GeTe_2 van der Waals heterostructure, Nat. Commun. **11**, 3860 (2020).

[11] F. Hellman, A. Hoffmann, Y. Tserkovnyak, G. S. D. Beach, E. E. Fullerton, C. Leighton, A. H. MacDonald, D. C. Ralph, D. A. Arena, and H. A. Dürr, Interface-induced phenomena in magnetism, Rev. Mod. Phys. **89**, 025006 (2017).

[12] S. S. P. Parkin, M. Hayashi, and L. Thomas, Magnetic domain-wall racetrack memory, Science **320**, 190 (2008).

[13] P. A. Joy and S. Vasudevan, Magnetism in the layered transition-metal thiophosphates MPS_3 (M = Mn, Fe, and Ni), Phys. Rev. B **46**, 5425 (1992).

[14] E. Ergeçen, B. Ilyas, J. Kim, J. Park, M. B. Yilmaz, T. Luo, D. Xiao, S. Okamoto, J.-G. Park, and N. Gedik, Coherent detection of hidden spin–lattice coupling in a van der Waals antiferromagnet, Proc. Natl. Acad. Sci. **120**, e2208968120 (2023).

[15] M. Gibertini, M. Koperski, A. F. Morpurgo, and K. S. Novoselov, Magnetic 2D materials and heterostructures, Nat. Nanotechnol. **14**, 408 (2019).

[16] C.-Z. Chang, Marriage of topology and magnetism, Nat. Mater. **19**, 484 (2020).

[17] W. Zhao, Z. Fei, T. Song, H. K. Choi, T. Palomaki, B. Sun, P. Malinowski, M. A. McGuire, J.-H. Chu, and X. Xu, Magnetic

proximity and nonreciprocal current switching in a monolayer WTe_2 helical edge, Nat. Mater. **19**, 503 (2020).

[18] N. K. Singh, D. Rawat, D. Dey, A. Elsukova, P. O. Å. Persson, P. Eklund, A. Taraphder, and A. Soni, Electron-phonon coupling and quantum correction to topological magnetoconductivity in Bi_2GeTe_4, Phys. Rev. B **105**, 045134 (2022).

[19] S. Paul, S. Karak, A. Mathew, A. Ram, and S. Saha, Electron-phonon and phonon-phonon anharmonic interactions in 2H−MoX_2 (X= S, Te): A Comprehensive Resonant Raman Study, Phys. Rev. B **104**, 075418 (2021).

[20] X. Cong, X.-L. Liu, M.-L. Lin, and P.-H. Tan, Application of raman spectroscopy to probe fundamental properties of two-dimensional materials, npj 2D Mater. Appl. **4**, 13 (2020).

[21] C. Liu, Z. Li, J. Hu, H. Duan, C. Wang, L. Cai, S. Feng, Y. Wang, R. Liu, and D. Hou, Probing the Néel-type antiferromagnetic order and coherent magnon-exciton coupling in van der Waals VPS_3, Adv. Mater. 2300247 (2023).

[22] J.-U. Lee, S. Lee, J. H. Ryoo, S. Kang, T. Y. Kim, P. Kim, C.-H. Park, J.-G. Park, and H. Cheong, Ising-type magnetic ordering in atomically thin $FePS_3$, Nano Lett. **16**, 7433 (2016).

[23] K. Kim, S. Y. Lim, J.-U. Lee, S. Lee, T. Y. Kim, K. Park, G. S. Jeon, C.-H. Park, J.-G. Park, and H. Cheong, Suppression of magnetic ordering in XXZ-type antiferromagnetic monolayer $NiPS_3$, Nat. Commun. **10**, 345 (2019).

[24] Y.-J. Sun, Q.-H. Tan, X.-L. Liu, Y.-F. Gao, and J. Zhang, Probing the magnetic ordering of antiferromagnetic $MnPS_3$ by raman spectroscopy, J. Phys. Chem. Lett. **10**, 3087 (2019).

[25] See Supplemental Material at http://link.aps.org/supplemental/10.1103/PhysRevB.109.085136 for the Supplemental Material contains a detailed description of the preparation of the heterostructures, their characterization (by Raman, atomic force microscopy, and magnetization measurements), and discussions on the effect of strain, charge transfer, and interlayer coupling in the heterostructures.

[26] H.-J. Koo, R. Kremer, and M.-H. Whangbo, Unusual spin exchanges mediated by the molecular anion $P_2S_6^{4-}$: Theoretical analyses of the magnetic ground states, magnetic anisotropy and spin exchanges of MPS_3 (M = Mn, Fe, Co, Ni), Molecules **26**, 1410 (2021).

[27] G. Ouvrard, R. Brec, and J. Rouxel, Structural determination of some MPS_3 layered phases (M = Mn, Fe, Co, Ni and Cd), Mater. Res. Bull. **20**, 1181 (1985).

[28] K. Kurosawa, S. Saito, and Y. Yamaguchi, Neutron diffraction study on $MnPS_3$ and $FePS_3$, J. Phys. Soc. Jpn. **52**, 3919 (1983).

[29] D. Lançon, H. C. Walker, E. Ressouche, B. Ouladdiaf, K. C. Rule, G. J. McIntyre, T. J. Hicks, H. M. Rønnow, and A. R. Wildes, Magnetic structure and magnon dynamics of the quasi-two-dimensional antiferromagnet $FePS_3$, Phys. Rev. B **94**, 214407 (2016).

[30] M. J. Coak, D. M. Jarvis, H. Hamidov, A. R. Wildes, J. A. M. Paddison, C. Liu, C. R. S. Haines, N. T. Dang, S. E. Kichanov, and B. N. Savenko, Emergent magnetic phases in pressure-tuned van der Waals antiferromagnet $FePS_3$, Phys. Rev. X **11**, 011024 (2021).

[31] A. R. Wildes, V. Simonet, E. Ressouche, G. J. Mcintyre, M. Avdeev, E. Suard, S. A. J. Kimber, D. Lançon, G. Pepe, and B. Moubaraki, Magnetic structure of the quasi-two-dimensional antiferromagnet $NiPS_3$, Phys. Rev. B **92**, 224408 (2015).

[32] T. Y. Kim and C.-H. Park, Magnetic anisotropy and magnetic ordering of transition-metal phosphorus trisulfides, Nano Lett. **21**, 10114 (2021).

[33] L. Du, J. Tang, Y. Zhao, X. Li, R. Yang, X. Hu, X. Bai, X. Wang, K. Watanabe, and T. Taniguchi, Lattice dynamics, phonon chirality, and spin–phonon coupling in 2D itinerant ferromagnet Fe_3GeTe_2, Adv. Funct. Mater. **29**, 1904734 (2019).

[34] D. Vaclavkova, A. Delhomme, C. Faugeras, M. Potemski, A. Bogucki, J. Suffczyński, P. Kossacki, A. R. Wildes, B. Grémaud, and A. Saúl, Magnetoelastic interaction in the two-dimensional magnetic material $MnPS_3$ studied by first principles calculations and Raman experiments, 2D Mater. **7**, 035030 (2020).

[35] S. Paul, S. Karak, M. Mandal, A. Ram, S. Marik, R. P. Singh, and S. Saha, Tailoring the phase transition and electron-phonon coupling in $1T'$-$MoTe_2$ by charge doping: A Raman study, Phys. Rev. B **102**, 054103 (2020).

[36] S. Paul, S. Talukdar, R. S. Singh, and S. Saha, Topological phase transition in $MoTe_2$: A review, Phys. Status Solidi (RRL) **17**, 2200420 (2023).

[37] K. Zhang, C. Bao, Q. Gu, X. Ren, H. Zhang, K. Deng, Y. Wu, Y. Li, J. Feng, and S. Zhou, Raman signatures of inversion symmetry breaking and structural phase transition in type-II Weyl semimetal $MoTe_2$, Nat. Commun. **7**, 13552 (2016).

[38] N. D. Mermin and H. Wagner, Absence of ferromagnetism or antiferromagnetism in one-or two-dimensional isotropic Heisenberg models, Phys. Rev. Lett. **17**, 1133 (1966).

[39] P. C. Hohenberg, Existence of long-range order in one and two dimensions, Phys. Rev. **158**, 383 (1967).

[40] N. Chandrasekharan and S. Vasudevan, Magnetism and exchange in the layered antiferromagnet $NiPS_3$, J. Phys.: Condens. Matter **6**, 4569 (1994).

[41] S. N. Neal, H.-S. Kim, K. A. Smith, A. V. Haglund, D. G. Mandrus, H. A. Bechtel, G. L. Carr, K. Haule, D. Vanderbilt, and J. L. Musfeldt, Near-field infrared spectroscopy of monolayer $MnPS_3$, Phys. Rev. B **100**, 075428 (2019).

[42] S. N. Neal, H.-S. Kim, K. R. O'Neal, A. V. Haglund, K. A. Smith, D. G. Mandrus, H. A. Bechtel, G. L. Carr, K. Haule, and D. Vanderbilt, Symmetry crossover in layered MPS_3 complexes (M = Mn, Fe, Ni) via near-field infrared spectroscopy, Phys. Rev. B **102**, 085408 (2020).

[43] B. L. Chittari, Y. Park, D. Lee, M. Han, A. H. MacDonald, E. Hwang, and J. Jung, Electronic and magnetic properties of single-layer MPX_3 metal phosphorous trichalcogenides, Phys. Rev. B **94**, 184428 (2016).

[44] X. Ling, W. Fang, Y.-H. Lee, P. T. Araujo, X. Zhang, J. F. Rodriguez-Nieva, Y. Lin, J. Zhang, J. Kong, and M. S. Dresselhaus, Raman enhancement effect on two-dimensional layered materials: Graphene, h-BN and MoS_2, Nano Lett. **14**, 3033 (2014).

[45] I. Dzyaloshinsky, A thermodynamic theory of "weak" ferromagnetism of antiferromagnetics, J. Phys. Chem. Solids **4**, 241 (1958).

[46] T. Moriya, Anisotropic superexchange interaction and weak ferromagnetism, Phys. Rev. **120**, 91 (1960).

[47] Y. A. Bychkov and É. I. Rashba, Properties of a 2D electron gas with lifted spectral degeneracy, JETP Lett. **39**, 66 (1984).

[48] H. Yang, G. Chen, A. A. C. Cotta, A. T. N'Diaye, S. A. Nikolaev, E. A. Soares, W. A. A. Macedo, K. Liu, A. K. Schmid, and A. Fert, Significant Dzyaloshinskii–Moriya interaction at graphene–ferromagnet interfaces due to the Rashba effect, Nat. Mater. **17**, 605 (2018).

[49] T. Koretsune, N. Nagaosa, and R. Arita, Control of dzyaloshinskii-moriya interaction in $Mn_{1-x}Fe_xGe$: A first-principles study, Sci. Rep. **5**, 1 (2015).

[50] G. Nicolay, F. Reinert, S. Hüfner, and P. Blaha, Spin-orbit splitting of the L-gap surface state on Au(111) and Ag(111), Phys. Rev. B **65**, 033407 (2001).

[51] A. Tamai, W. Meevasana, P. D. C. King, C. W. Nicholson, A. De La Torre, E. Rozbicki, and F. Baumberger, Spin-orbit splitting of the Shockley surface state on Cu(111), Phys. Rev. B **87**, 075113 (2013).

[52] M. Charilaou and F. Hellman, Roughness effects in uncompensated antiferromagnets, J. Appl. Phys. **117**, 83907 (2015).

[53] M. Charilaou and F. Hellman, Surface-induced phenomena in uncompensated collinear antiferromagnets, J. Phys.: Condens. Matter **27**, 086001 (2015).

[54] M. Charilaou and F. Hellman, Anomalous magnetic thermodynamics in uncompensated collinear antiferromagnets, Europhys. Lett. **107**, 27002 (2014).

[55] B. Yamina and O. Abdelouahab, Geometries and electronic structures by DFT simulated annealing study of some noble metal small size clusters, Der Pharma Chem. **9**, 62 (2017).